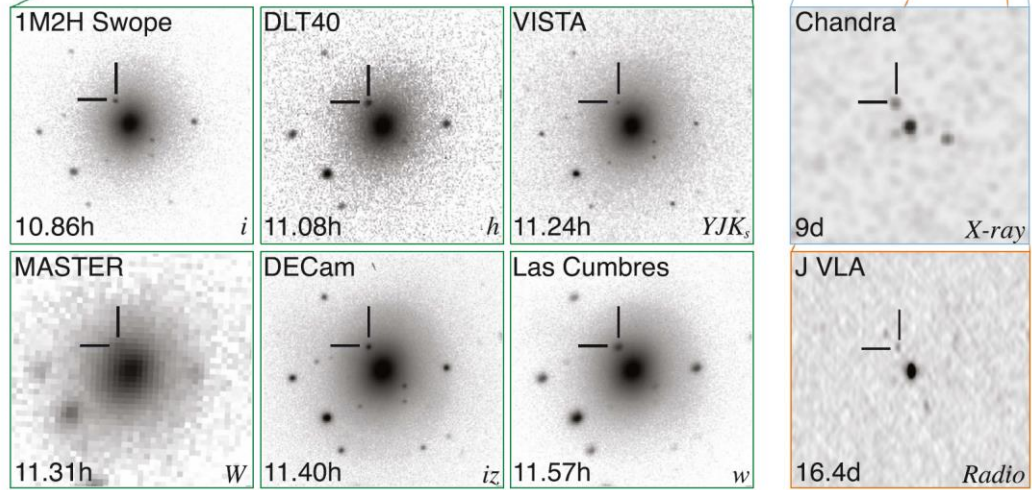
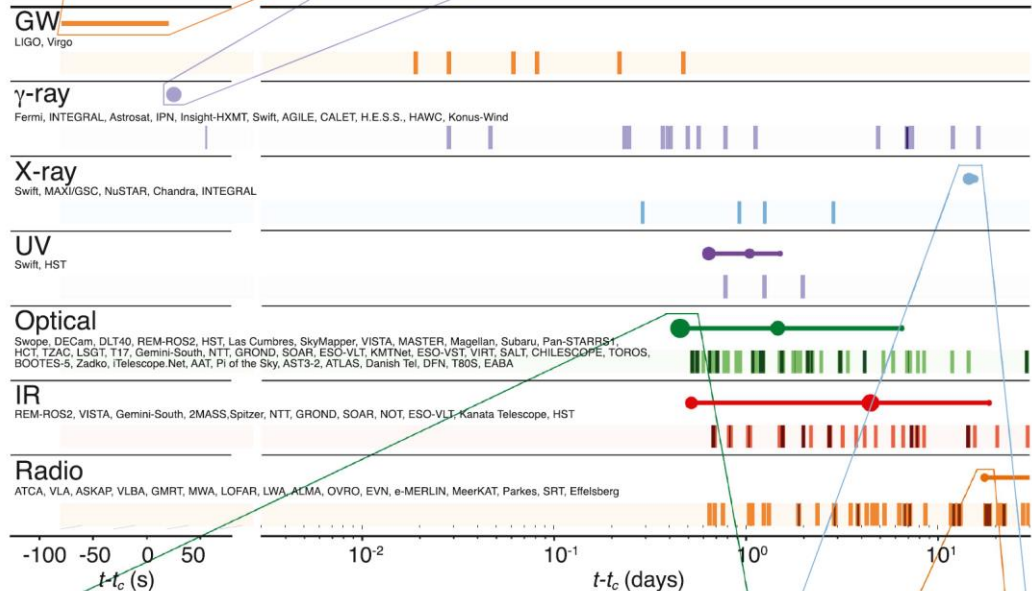
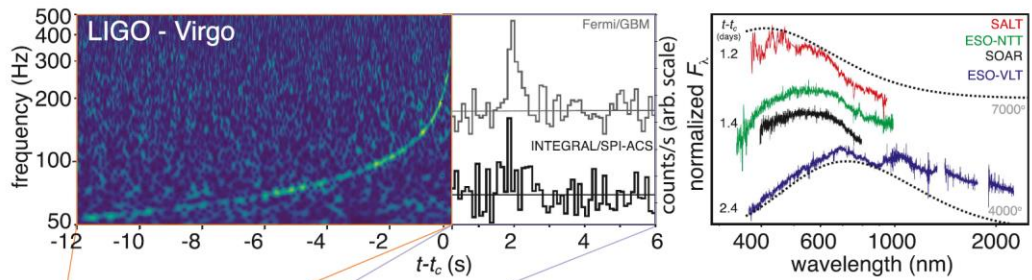


# Astrophysics of gravitational wave sources

Lecture 13: GW170817 & “future” sources of GW

Ondřej Pejcha

ÚTF MFF UK

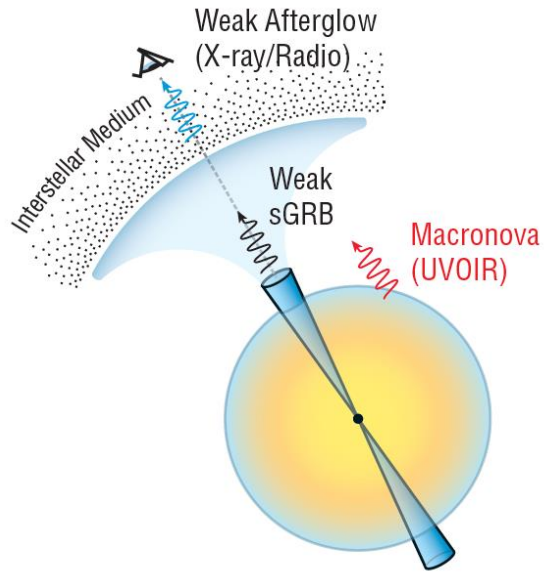


Abott et al. (2017)

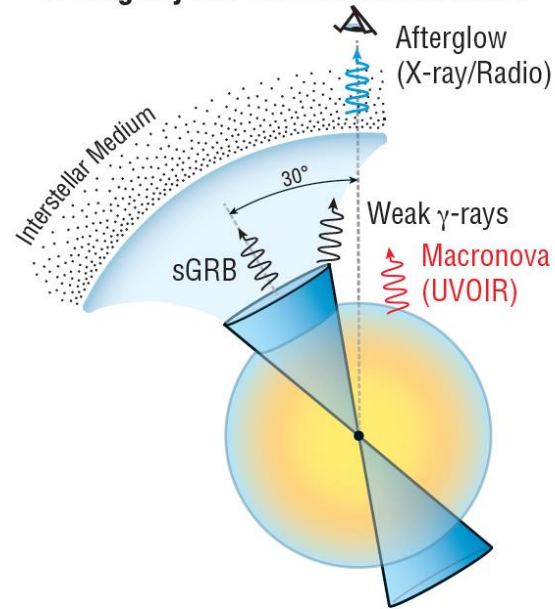
# Binary neutron star merger



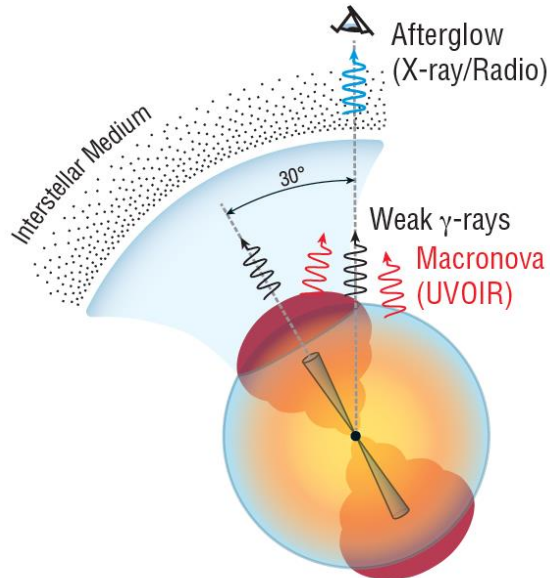
### A On-axis Weak sGRB



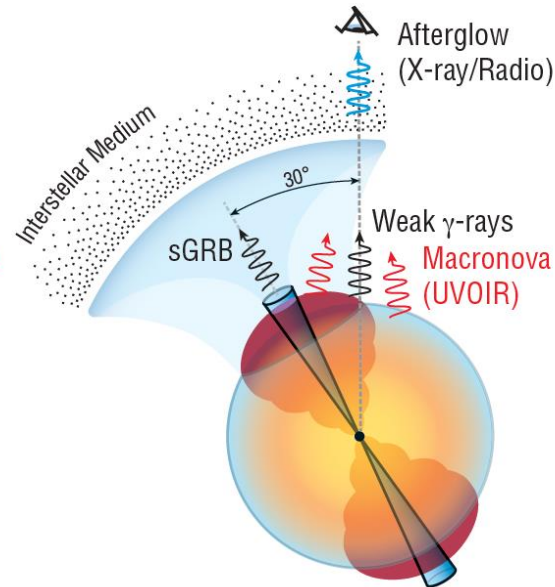
### B Slightly Off-Axis Classical sGRB

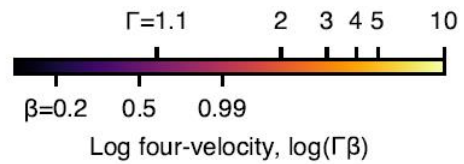
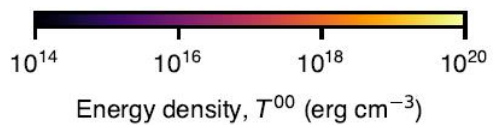
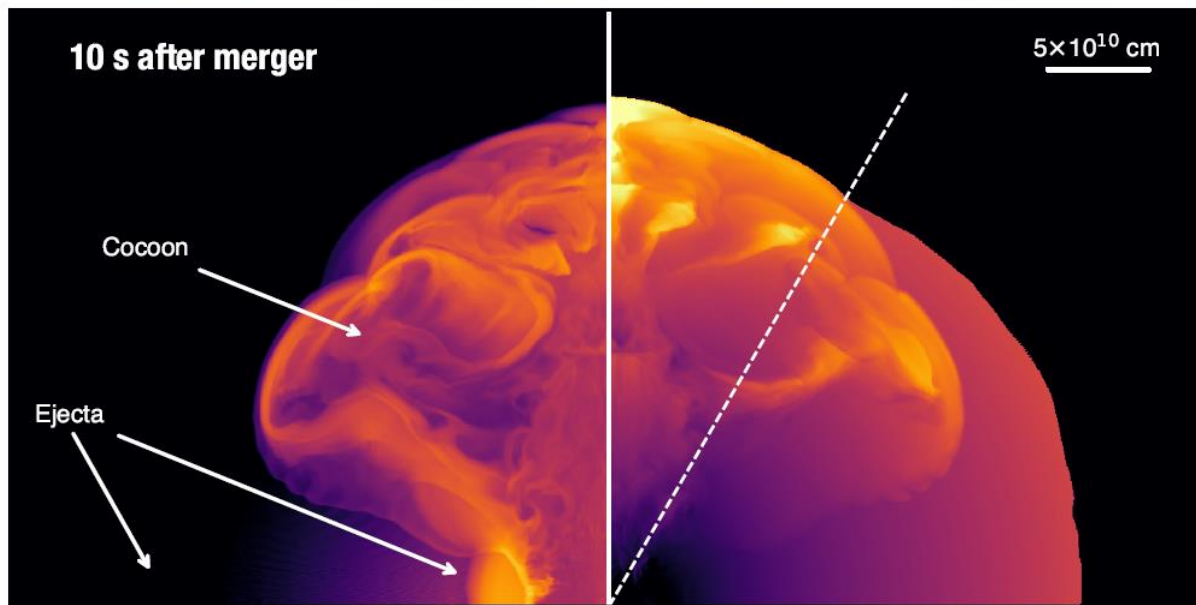
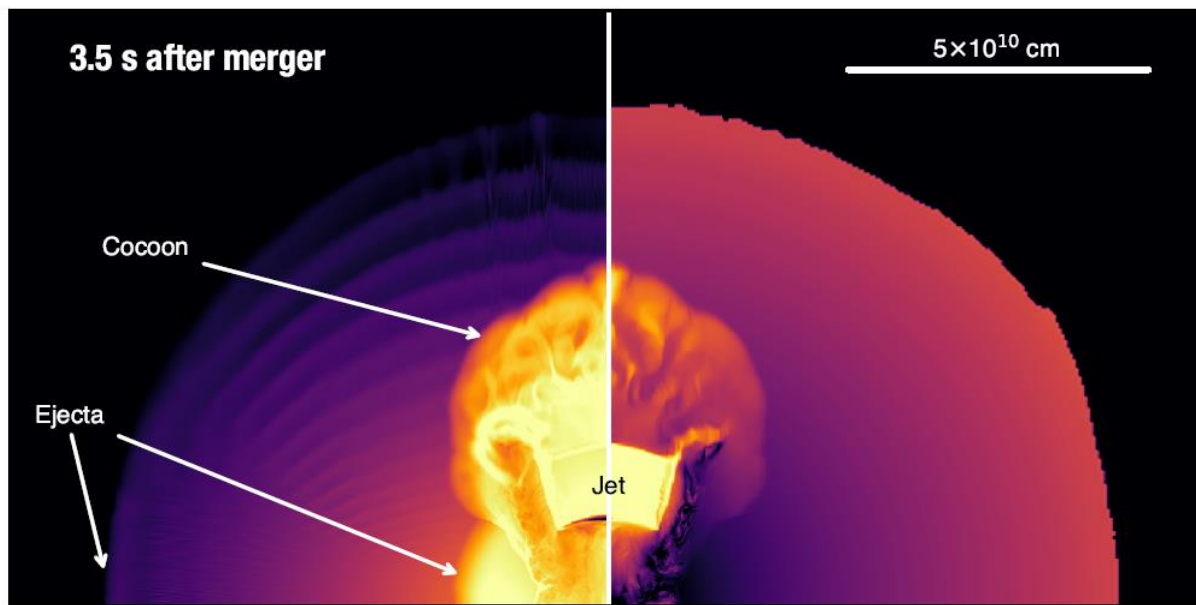


### C Cocoon with Choked Jet

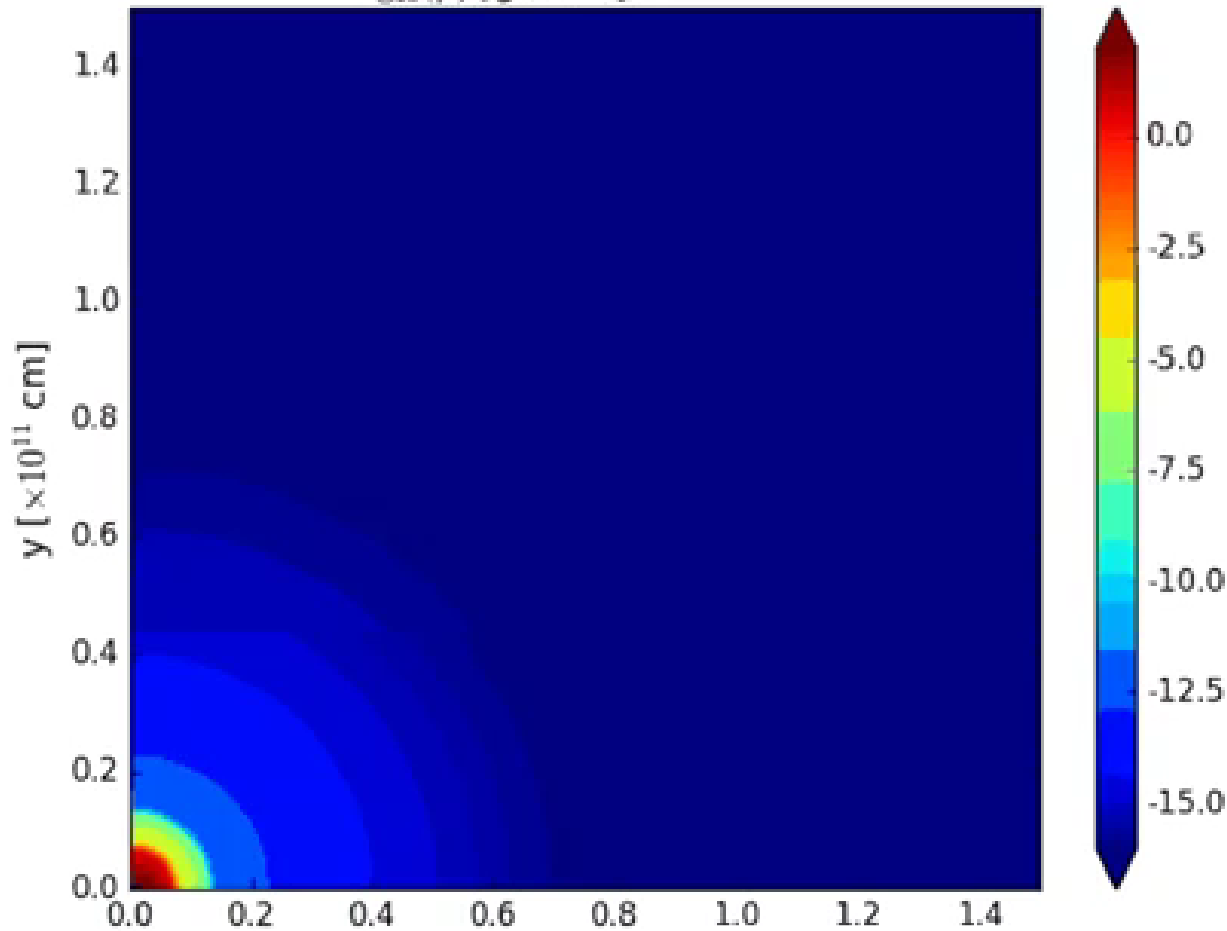


### D On-axis Cocoon with Off-Axis Jet





$\log_{10}(\rho)$  [gr/cm<sup>3</sup>], t=0.0 sec



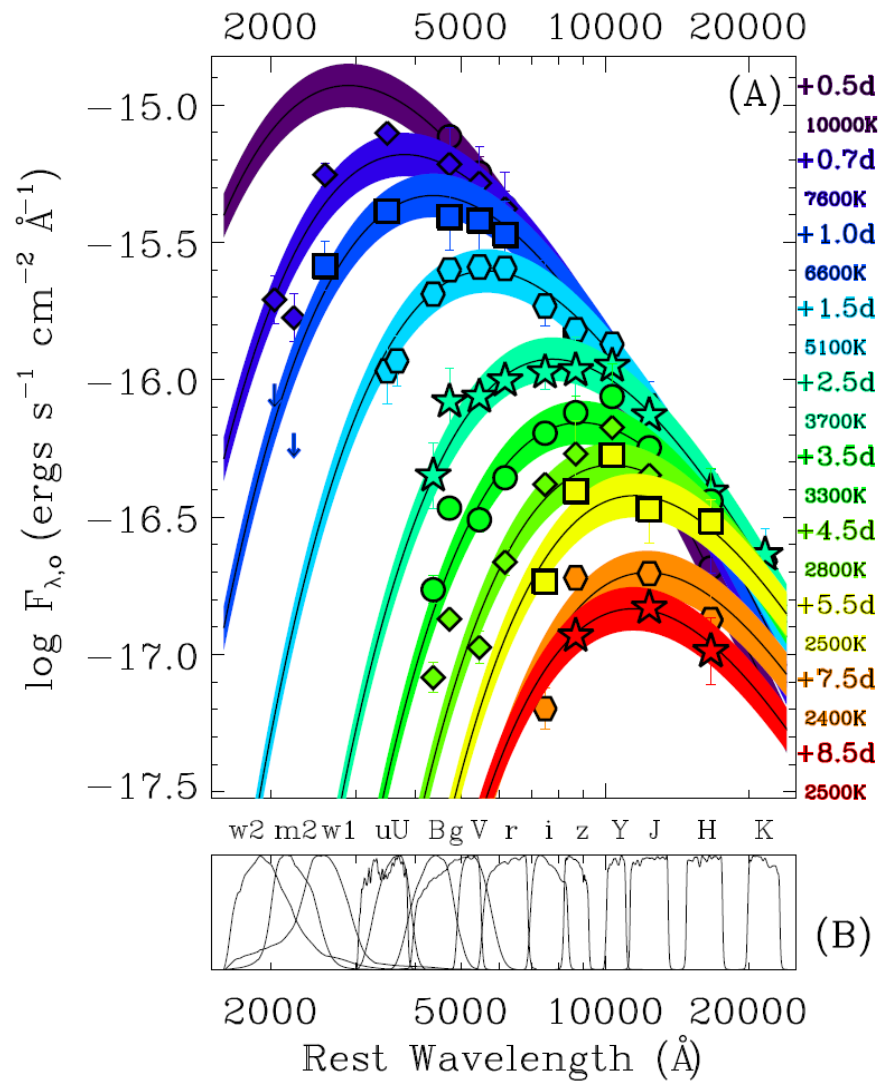
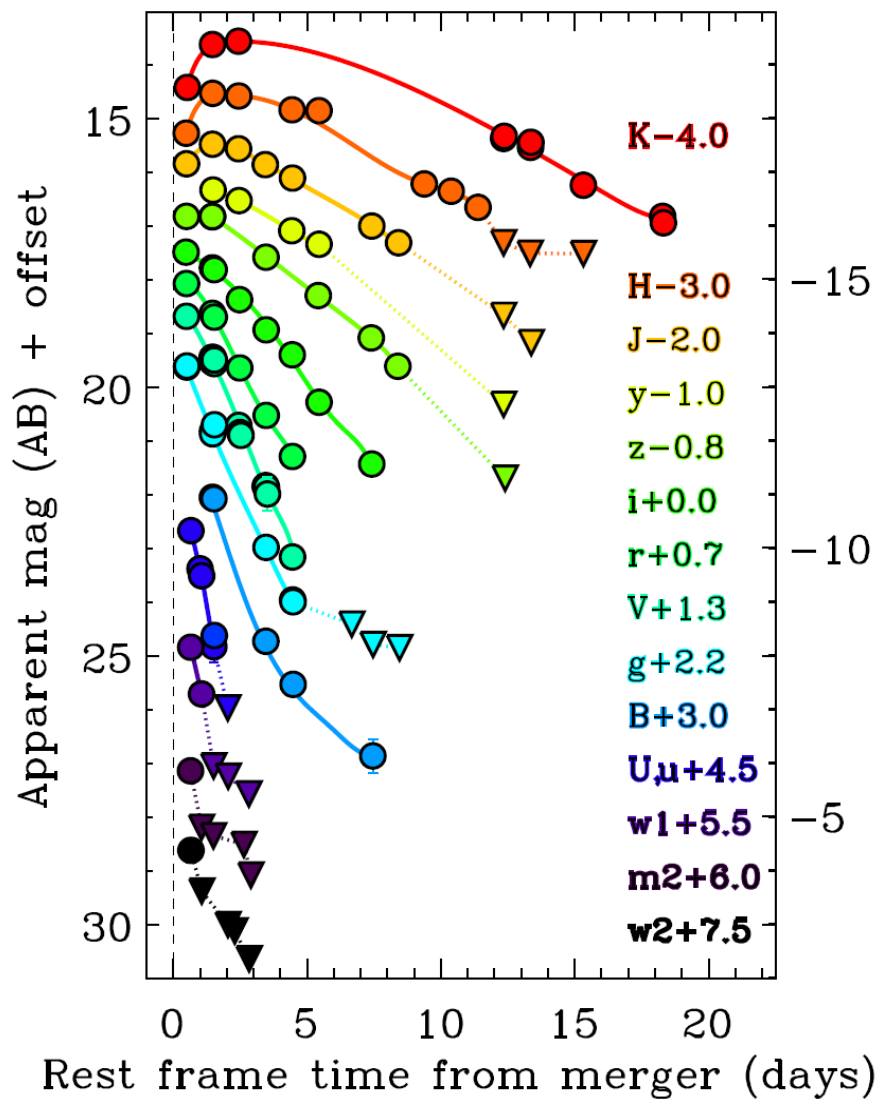
x [ $\times 10^{11}$  cm]

y [ $\times 10^{11}$  cm]

**ABSTRACT**

We present the first relativistic MHD numerical simulation of a magnetic jet that propagates through and emerges from the dynamical ejecta of a binary neutron star merger. Generated by the magnetized rotation of the merger remnant, the jet propagates through the ejecta and produces an energetic cocoon that expands at mildly relativistic velocities and breaks out of the ejecta. We show that if the ejecta has a low-mass ( $\sim 10^{-7} M_{\odot}$ ) high-velocity ( $v \sim 0.85 c$ ) tail, the cocoon shock breakout will generate  $\gamma$ -ray emission that is comparable to the observed short GRB170817A that accompanied the recent gravitational wave event GW170817. Thus, we propose that this GRB, which is quite different from all other short GRBs observed before, was produced by a different mechanism. We expect, however, that such events are numerous and many will be detected in coming LIGO-Virgo runs. **Bromberg et al. (2017)**

# Observations of GW170817



Drout et al. (2017)

$$t_{\text{lc}} \approx \left( \frac{3\kappa M}{4\pi c v} \right)^{\frac{1}{2}} \approx 2.7 \text{ days} \times \left( \frac{M}{0.01M} \right)^{\frac{1}{2}} \left( \frac{v}{0.1c} \right)^{\frac{1}{2}} \left( \frac{\kappa}{1 \text{ cm}^2 \text{ g}^{-1}} \right)^{\frac{1}{2}} \quad (2)$$

The characteristic luminosity of the kilonova is approximately equal to the radioactive heating rate at this escape timescale

$$L_{\text{lc}} \approx M \varepsilon_{\text{nuc}}(t_{\text{lc}}) \approx 5 \times 10^{40} \text{ erg s}^{-1} \times \left( \frac{M}{0.01M} \right)^{\frac{1}{2}} \left( \frac{v}{0.1c} \right)^{\frac{\alpha}{2}} \left( \frac{\kappa}{1 \text{ cm}^2 \text{ g}^{-1}} \right)^{-\frac{\alpha}{2}} \quad (3)$$

A larger ejecta mass produces a brighter and longer-lasting kilonova; a higher velocity gives a brighter and briefer kilonova.

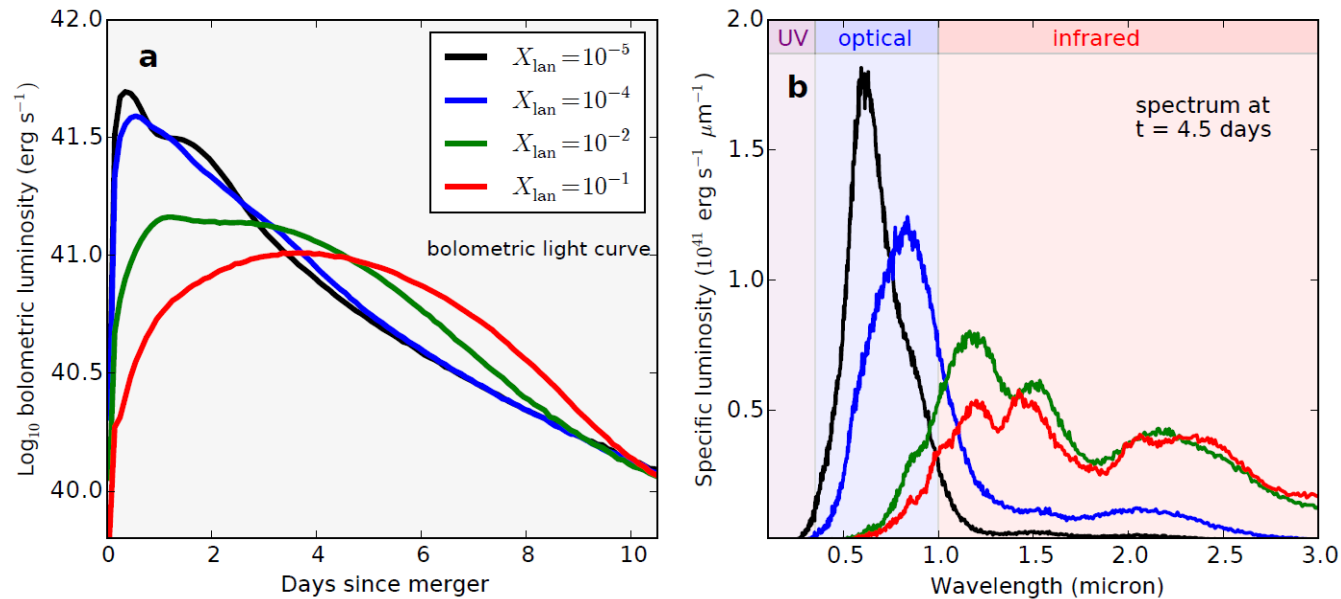


**Figure 2 | Models of kilonovae demonstrating the observable signatures of r-process abundances.** All models have an ejecta mass  $M = 0.05M_{\odot}$  and velocity  $v_k = 0.2c$ , but different mass fractions of lanthanides  $X_{\text{lan}}$ . **a**, Model bolometric light curves. If the ejecta is composed primarily of heavier r-process material ( $X_{\text{lan}} \geq 10^{-2}$ ) the opacity is higher, resulting in a longer diffusion times and longer duration bolometric light curves. **b**, Model spectra as observed 4.5 d after the mergers. The higher lanthanide opacities of the heavy r-process materials obscure the optical bands and shift the emission primarily to the infrared.

## Observable signatures of heavy element formation



# What can we learn from a spectrum of kilonova?

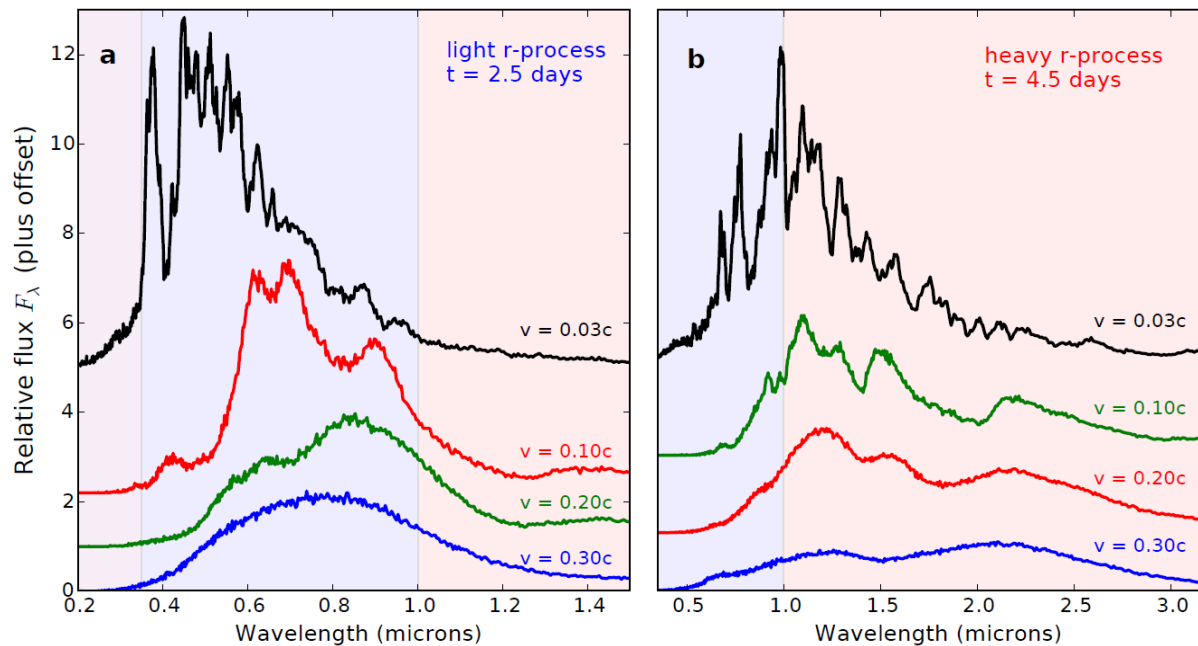


**Figure 3 | Models of kilonovae demonstrating the spectral diagnostics of the ejecta velocity.** The models all have ejecta mass  $M = 0.03M_\odot$ . **a**, Spectra of models composed of light r-process material ( $X_{\text{lan}} = 10^{-4}$ ) observed 1.5 d after the merger. Modest ejecta velocities ( $v_k = 0.03c$ , typical of supernovae) produce conspicuous absorption spectral features. At higher velocities ( $v_k = 0.1c$ – $0.2c$ ) the features are broadened and blended, while for  $v_k = 0.3c$  the spectra are essentially featureless. The optical spectra of AT 2017gfo were featureless, implying a high-velocity, approximately  $0.3c$  component of light r-process ejecta. **b**, Spectra of models composed of heavy r-process material ( $X_{\text{lan}} = 10^{-2}$ ) observed 3.5 d after the merger. The infrared spectra of AT 2017gfo showed broad peaks, implying a lower-velocity, approximately  $0.1c$  component of heavy r-process ejecta.

# What can we learn from a spectrum of kilonova?

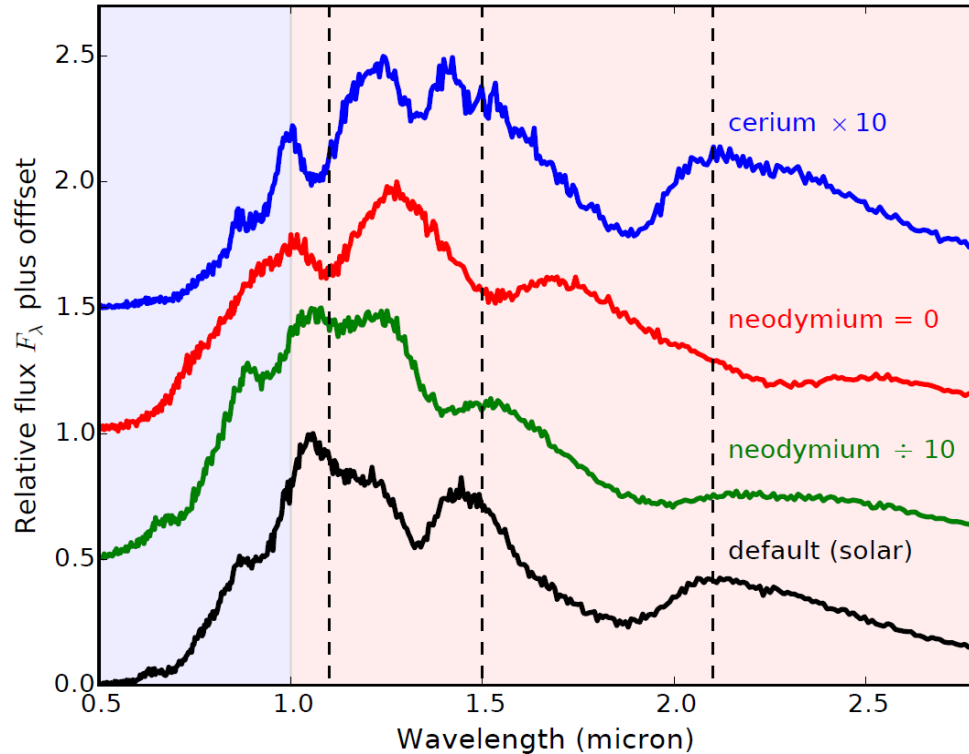
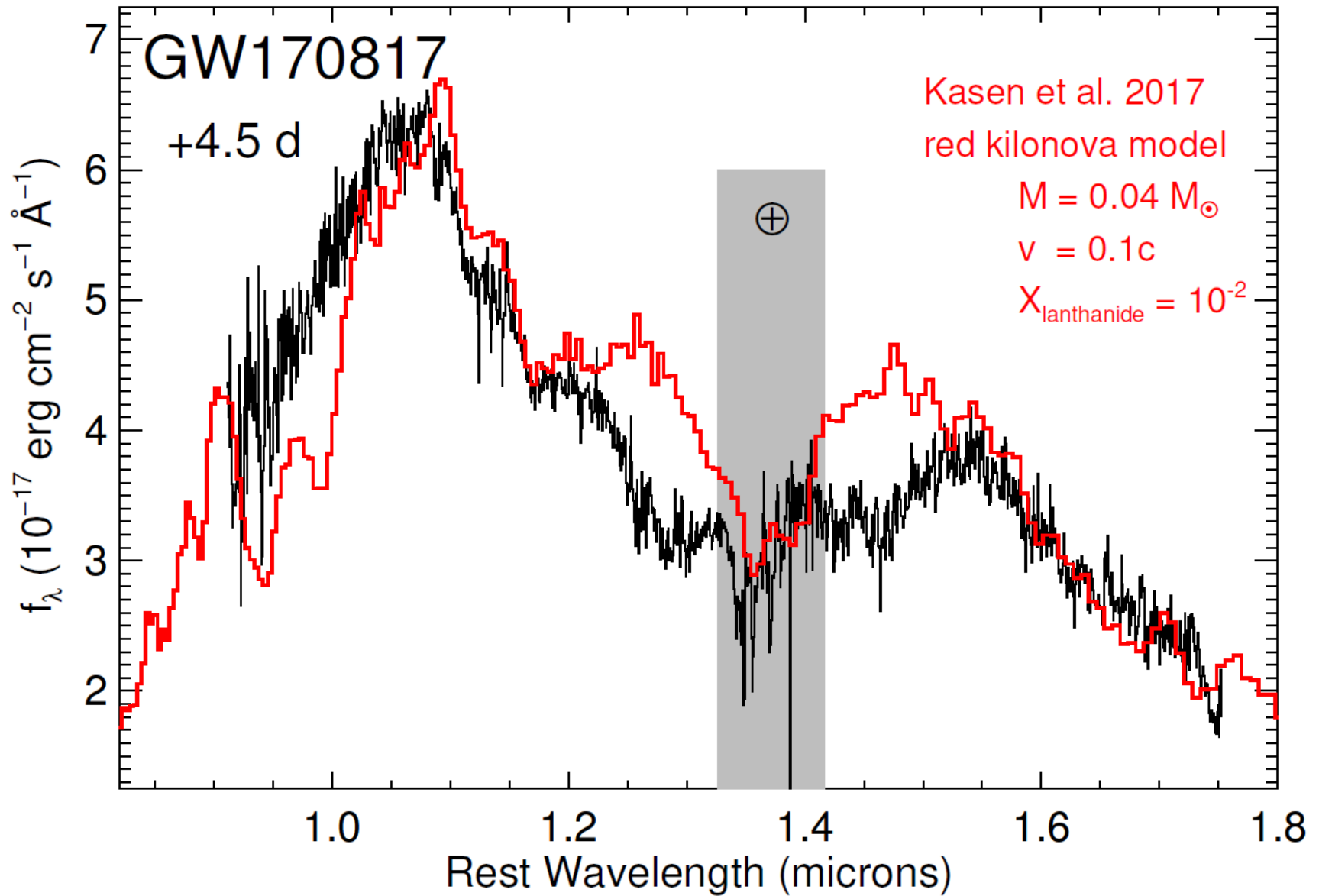
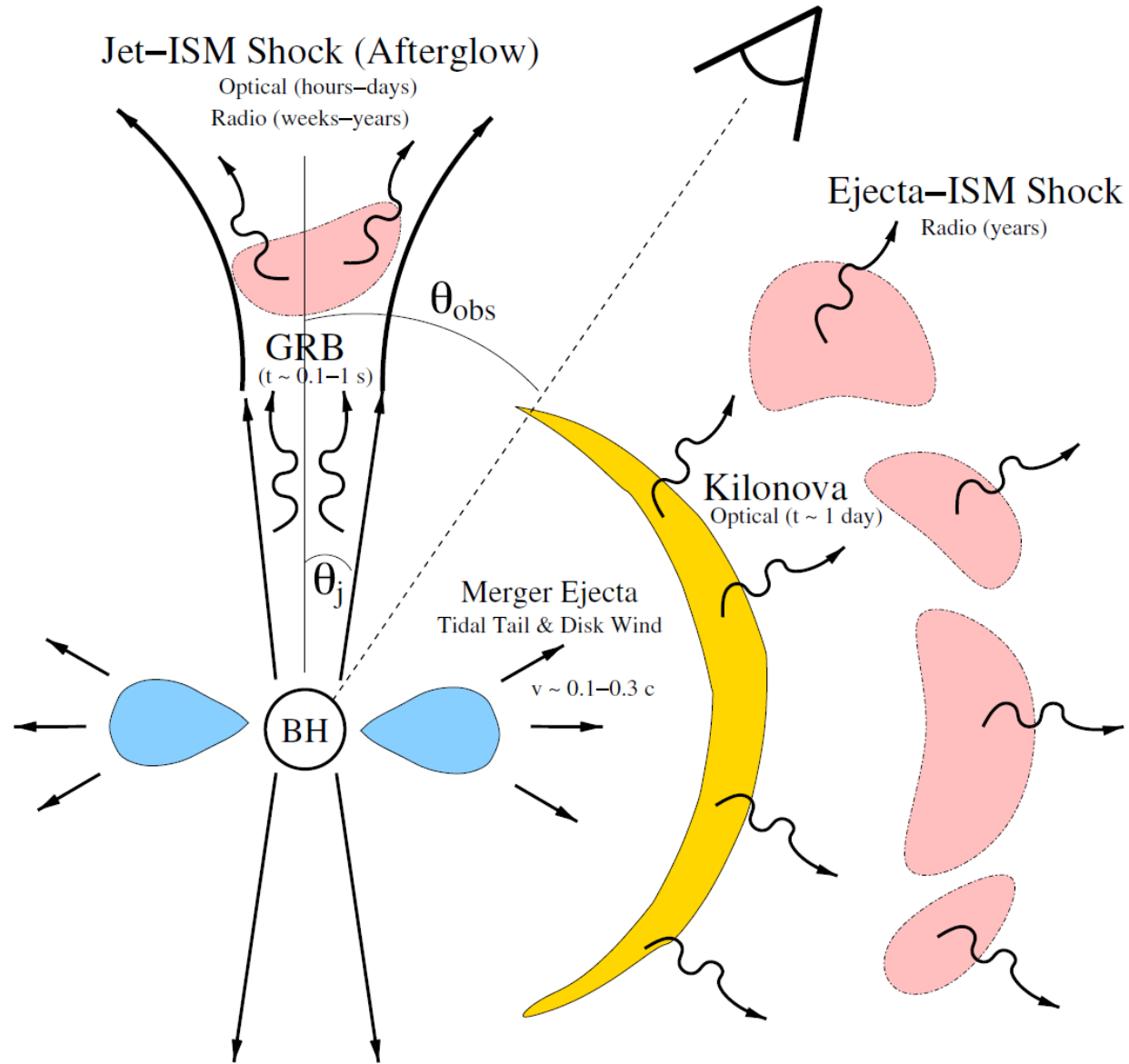


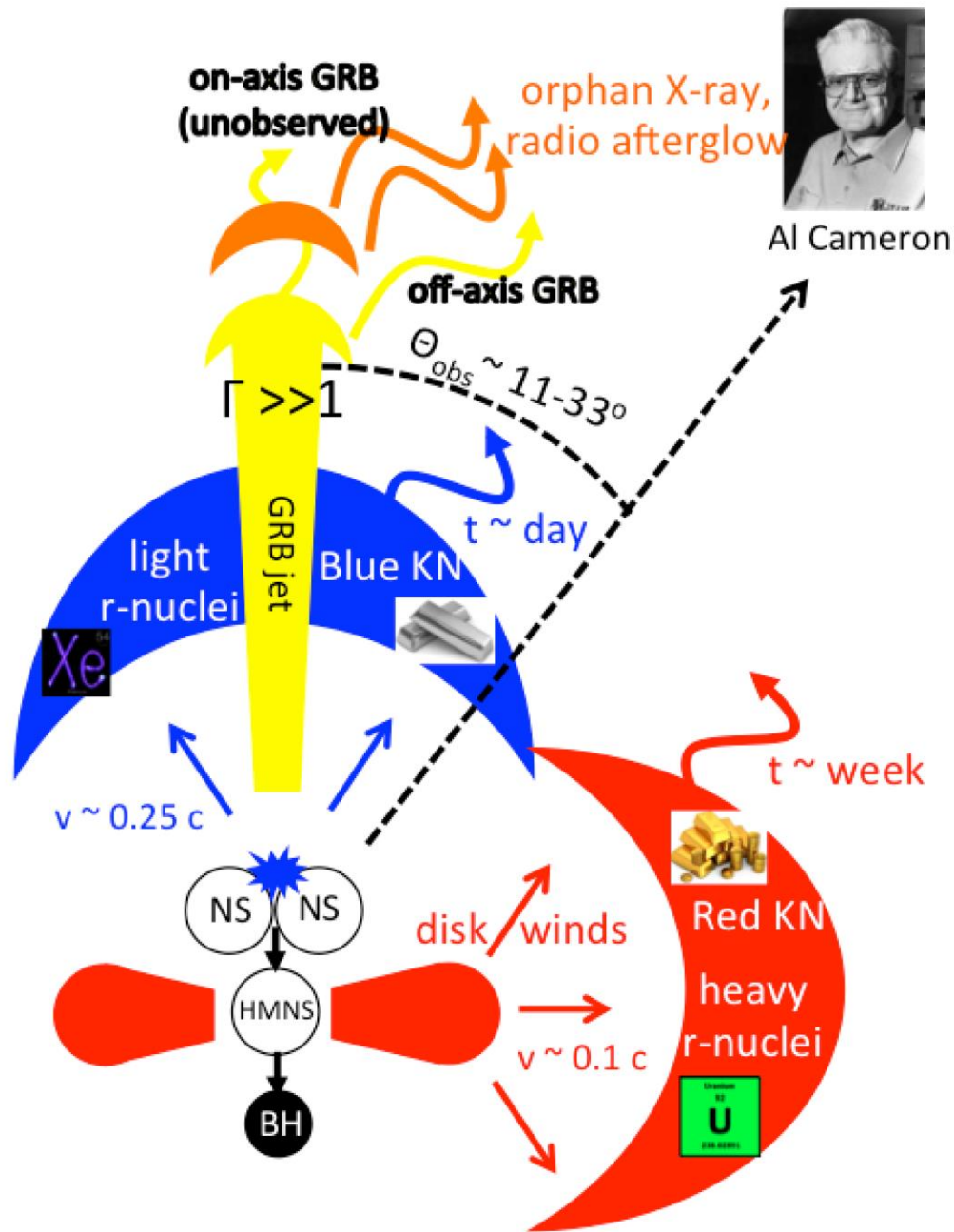
**Figure 4 | Models demonstrating how kilonova spectral features probe the abundance of individual r-process elements.** The spectral peaks in the models are blends of many lines, primarily those of the complex lanthanide species. The default model shown (parameters  $M = 0.04M_\odot$ ,  $v_k = 0.15c$ ,  $X_{\text{lan}} = 10^{-1.5}$ ) uses a solar distribution of lanthanides, and has spectral peaks near 1.1  $\mu\text{m}$ , 1.5  $\mu\text{m}$  and 2.0  $\mu\text{m}$  (marked with dashed lines). These features are mainly attributable to neodymium ( $Z = 60$ ) given that reducing or removing this species changes the feature locations. However, other lanthanides such as cerium ( $Z = 58$ ) also affect the blended peaks. Uncertainties in the current atomic line data sources limit hinder spectral analysis, but with improved atomic inputs a more detailed compositional breakdown is within reach.

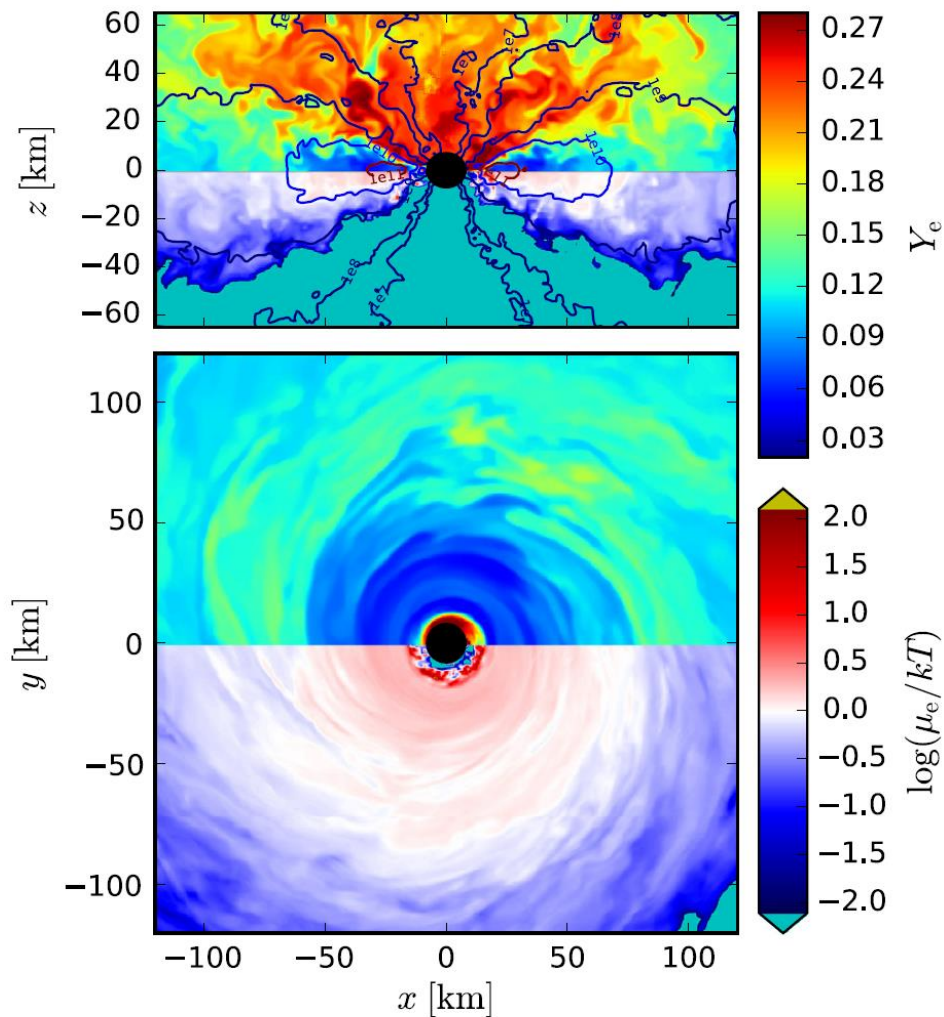
# Observations of GW170817



# Neutron star mergers

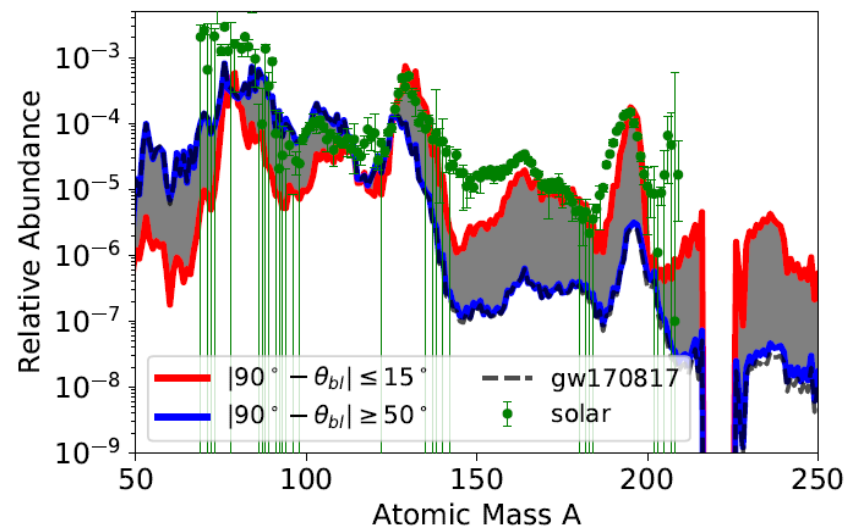
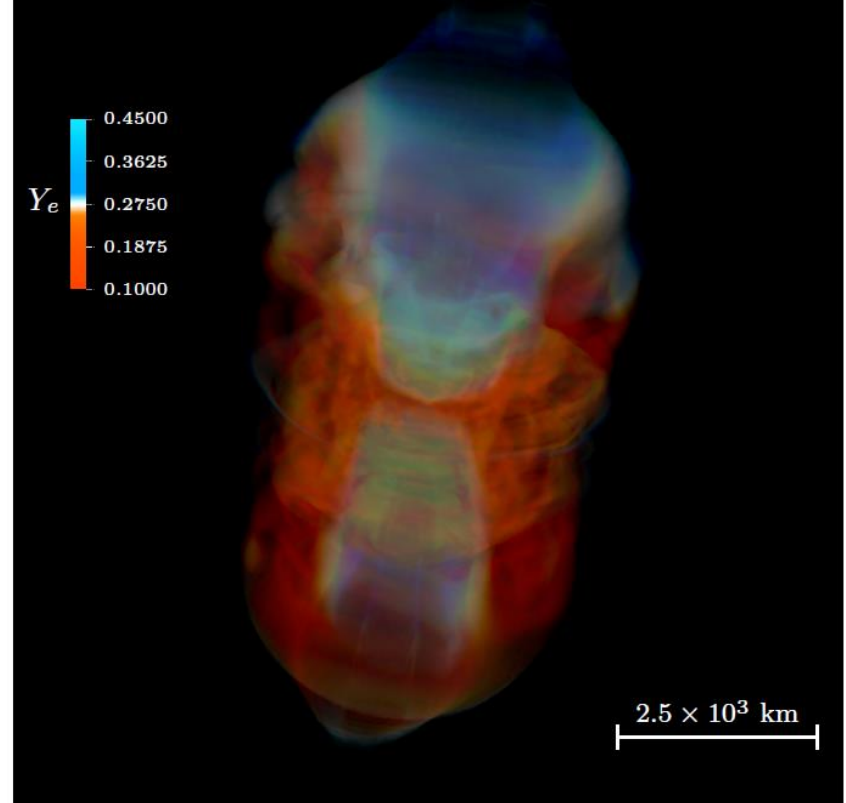






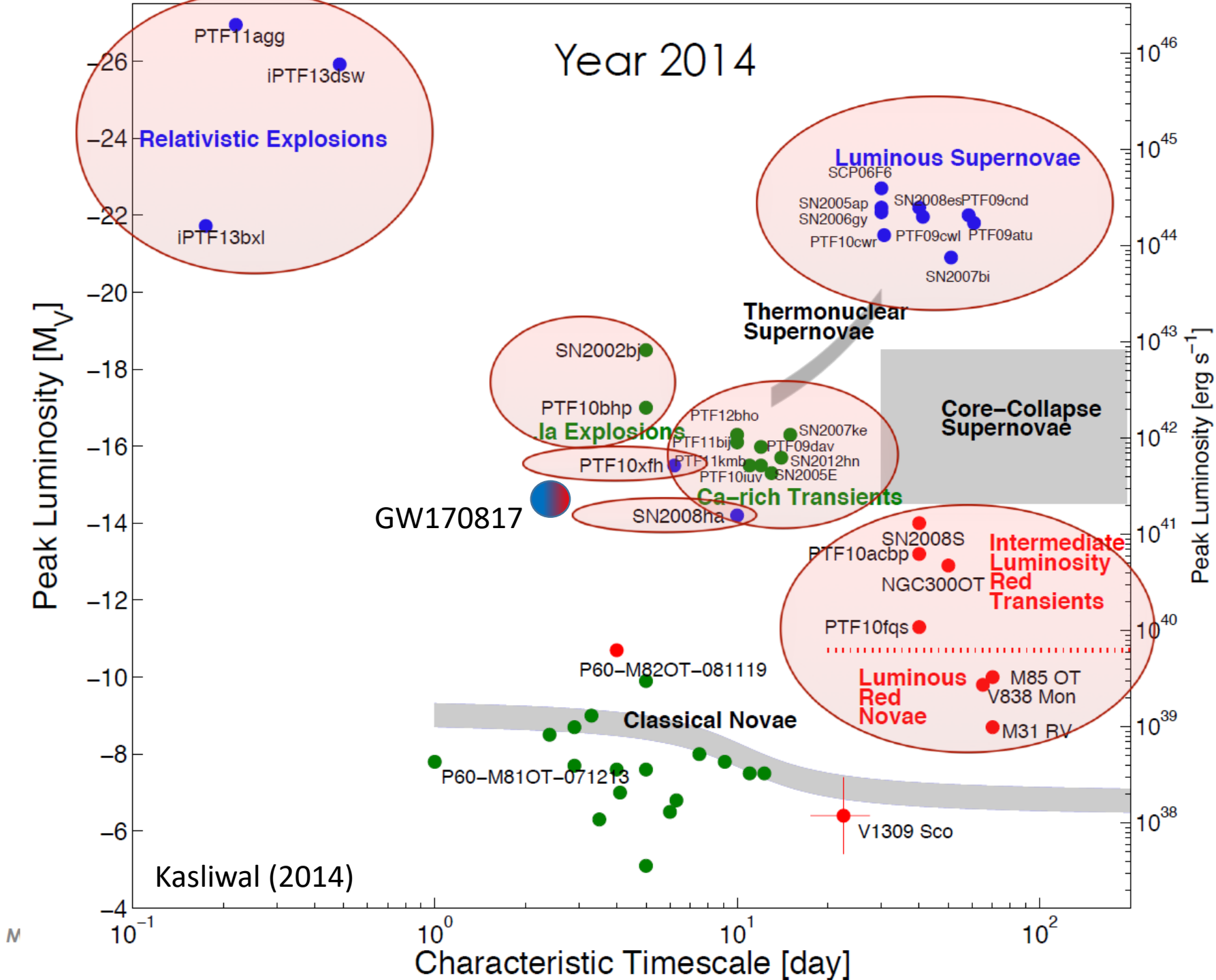
Over the 380-ms duration of the simulation, we find that a fraction  $\approx 20\%$  of the initial torus mass is unbound in powerful outflows with asymptotic velocities  $v \approx 0.1c$  and electron fractions  $Y_e \approx 0.1-0.25$ .

Siegel & Metzger (2017)

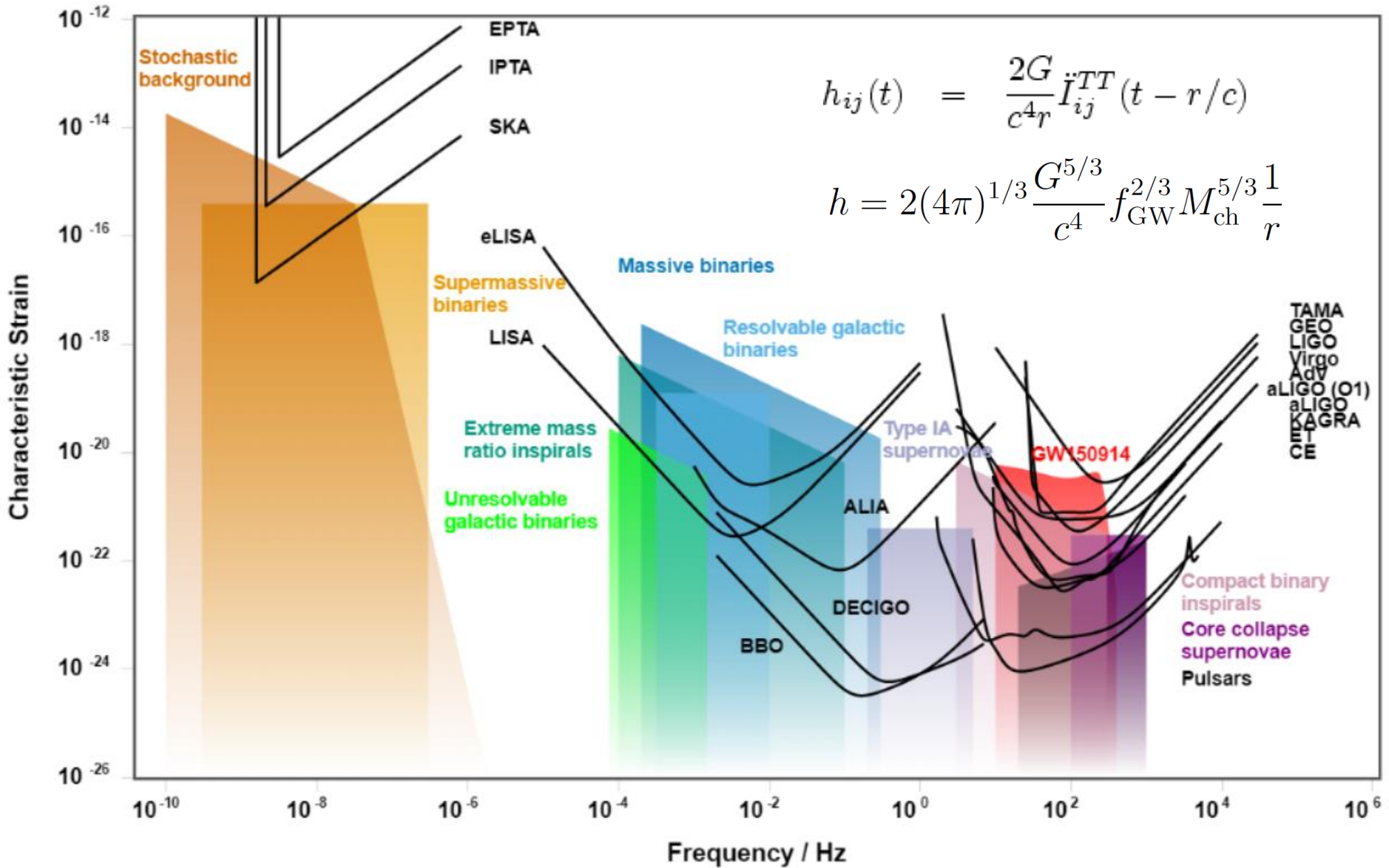


Miller et al. (2019)

Year 2014



# Gravitational Wave Detectors and Sources



$$h_{ij}(t) = \frac{2G}{c^4 r} \ddot{I}_{ij}^{TT}(t - r/c)$$

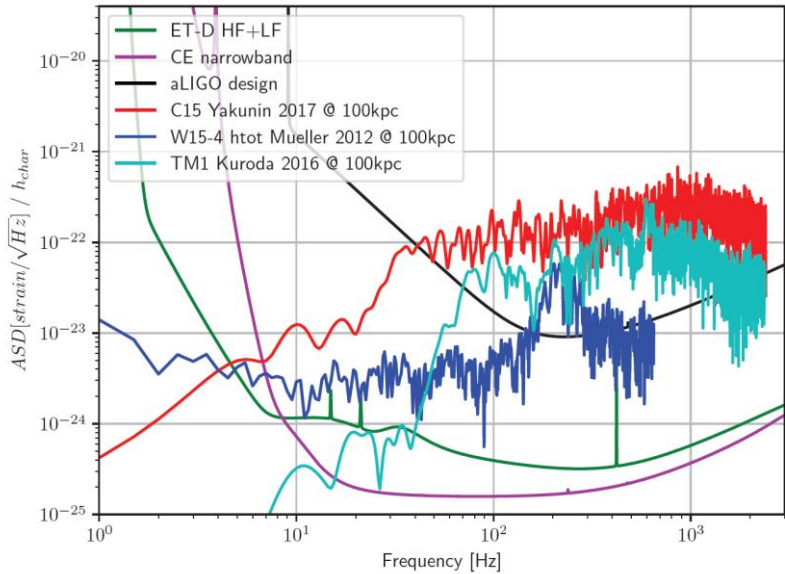
$$h = 2(4\pi)^{1/3} \frac{G^{5/3}}{c^4} f_{\text{GW}}^{2/3} M_{\text{ch}}^{5/3} \frac{1}{r}$$



# Binary objects

- Binary neutron stars / black holes
- White dwarfs
- EMRIs = Extreme Mass-ratio Inspirals
- Supermassive black holes

# Core-collapse supernovae



Kalogera et al. (2019)

GW also from accreting NS and other surface processes on NS

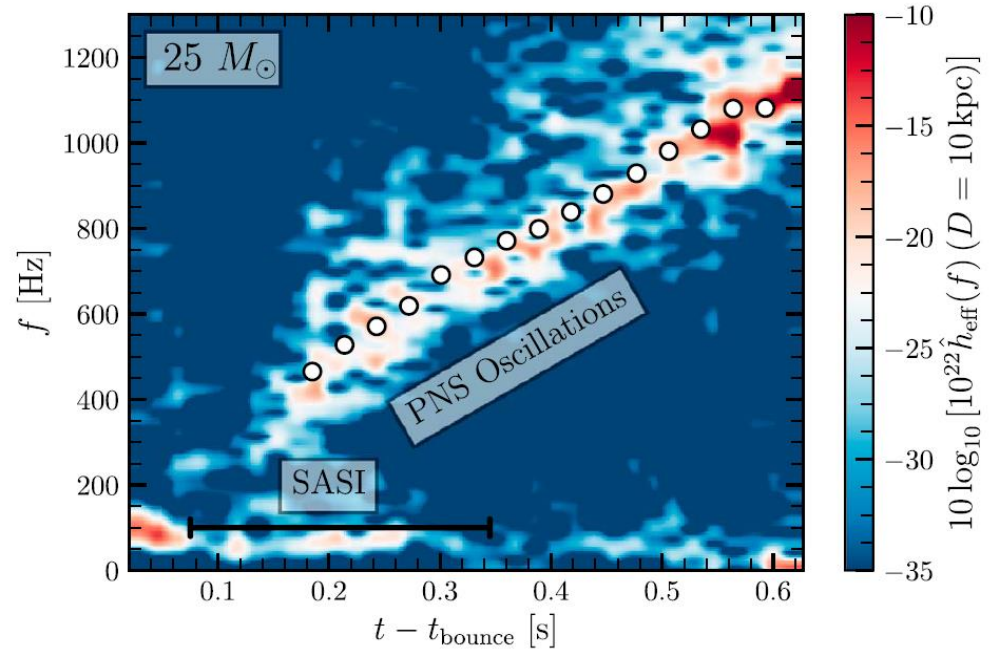


**Figure 5.** Time–frequency content of the GW signal for the  $25 M_{\odot}$  progenitor. The white dots denote the eigenfrequencies associated with the quadrupolar  $f$ - and low-order,  $n = 1, 2$ ,  $g$ -modes of the PNS as computed from linear perturbation theory. This progenitor is the only one in our set showing a clear signature of the SASI at low frequency. The presence of a higher-frequency component associated with PNS oscillations is instead universal.

Radice et al. (2019)

# Stochastic GW background

Unresolved sources of cosmological and astrophysical origin,  
redshifted accordingly to their emission epoch

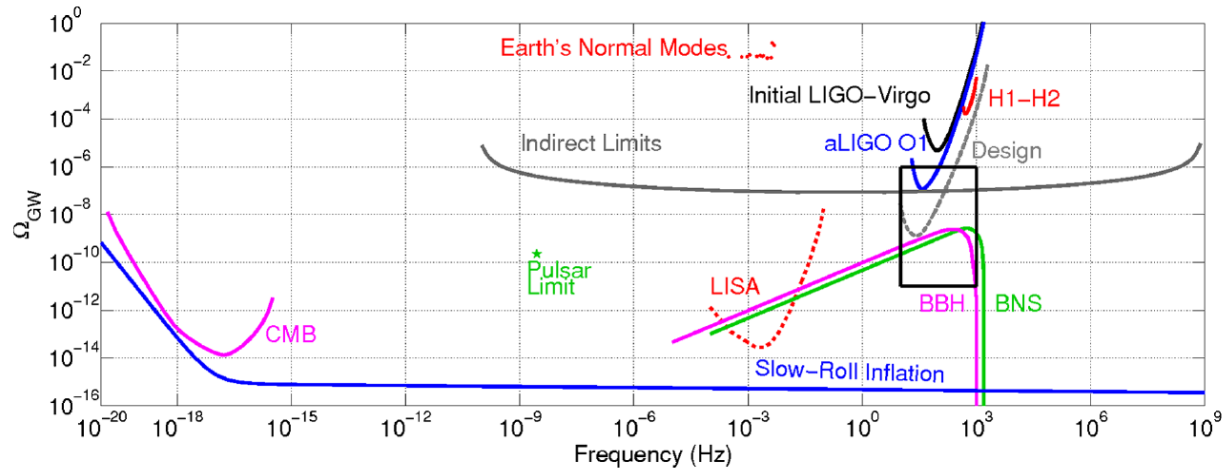


FIG. 3. Presented, here, are constraints on the background in PI form [59], as well as some representative models, across many decades in frequency. We compare the limits from ground-based interferometers from the final science run of Initial LIGO-Virgo, the colocated detectors at Hanford (H1–H2), Advanced LIGO (aLIGO) O1, and the projected design sensitivity of the advanced detector network assuming two years of coincident data, with constraints from other measurements: CMB measurements at low multipole moments [60], indirect limits from the cosmic microwave background (CMB) and big bang nucleosynthesis [61,62], pulsar timing [62], and from the ringing of Earth’s normal modes [63]. We also show projected limits from a space-based detector such as LISA [59,64,65], following the assumptions of [59]. We extend the BNS and BBH distributions using an  $f^{2/3}$  power-law down to low frequencies, with a low-frequency cutoff imposed where the inspiral time scale is of the order of the Hubble scale. In Fig. 5, we show the region in the black box in more detail.